Study of High-dose X-ray Radiation Damage of Silicon Sensors

Robert Klanner[a,*], Eckhart Fretwurst[a], Ioana Pintilie[b], Joern Schwandt[a], Jiaguo Zhang[a]

[a] *University of Hamburg, Hamburg, Germany*
[b] *National Institute of Materials Physics, Bucharest, Romania*

Abstract

The high intensity and high repetition rate of the European X-Ray Free-Electron Laser, presently under construction in Hamburg, will require pixel sensors which can stand X-ray doses up to 1 GGy for 3 years of operation. Within the AGIPD Collaboration the Hamburg group has systematically studied X-ray damage in silicon sensors for the dose range between 10 kGy and 1 GGy using strip sensors and test structures fabricated on high-ohmic *n*-type silicon from four different vendors. The densities of oxide charges, interface traps and surface current as function of dose and annealing conditions have been determined. The results have been implemented in TCAD simulations, and the radiation performance of strip sensors and guard-ring structures has been simulated and compared to experimental results. Finally, with the help of detailed TCAD simulations, the layout and technological parameters of the AGIPD pixel sensor have been optimized. It is found that the optimization for silicon sensors exposed to high X-ray doses is significantly different from that for non-irradiated sensors, and that the specifications of the AGIPD sensor can be met.

Keywords: XFEL, silicon pixel sensor, plasma effect, X-ray radiation damage, sensor optimization.

1. Introduction

The European X-Ray Free-Electron Laser (EuXFEL) [1, 2], planned to start operation in 2016, will provide X-ray beams with unique features: A brilliance which is 8 orders of magnitude higher than the most brilliant synchrotron-radiation beams for wavelengths in the Ångström region, full transverse coherence, a pulse length of about 10 fs, and pulse trains of 2700 pulses with 220 ns spacing every 100 ms. These unique features pose major challenges for imaging detectors, in particular [3, 4]: A dynamic range of 0, 1 to more than 10^4 photons of typically 12.4 keV per pixel, a radiation tolerance for doses up to 1 GGy for 3 years of operation, a good detection efficiency for X-rays with energies between 3 and 20 keV, and minimal inactive regions at the edge of the sensors.

Within the AGIPD (Adaptive Gain Integrating Pixel Detector) Collaboration [5, 6] the Hamburg group has studied the consequences of these requirements for p^+n-silicon sensors and optimized the design of the AGIPD sensor. From the study of the plasma effect, which occurs at high instantaneous X-ray densities [7, 8, 9], it has been concluded that, for a sensor of a thickness of 500 μm, an operating voltage above 500 V is needed to achieve a sufficiently high electric field to limit the spatial spread of the charge carriers and to achieve a charge-collection time compatible with the 220 ns spacing of the EuXFEL pulses. Studies of the charge collection in segmented sensors after irradiation with different X-ray doses [10, 11] have shown that, depending on X-ray dose, biasing history and environmental parameters like relative humidity, losses of holes or electrons occur. However, these effects have little relevance for the EuXFEL applications.

In this paper we summarize the results on the main effects of X-ray radiation damage, in particular the increase of oxide-charge density, the formation of Si-SiO_2-interface traps, their impact on dark current and breakdown voltage, and the optimization of the design of the AGIPD sensor for high operating voltages for X-ray doses between 0 and 1 GGy.

2. X-ray radiation damage of p^+n-silicon sensors

The X-ray energies at the EuXFEL are well below the threshold energy for the formation of defects in the silicon bulk, and only defects in the dielectric, at the Si-SiO_2 interface, and interfaces between dielectrics are generated. The effects of X-ray radiation damage are discussed in detail in [12, 13]. Here we give only a very short summary. In SiO_2 X-rays produce on average one *eh* pair every 18 eV of deposited energy. Depending on ionization density and electric field, a fraction of the *eh* pairs recombine. The remaining charge carriers move in the SiO_2 by diffusion and, if an electric field is present, by drift. Electrons, due to their high mobility and relatively low trapping probability, leave the SiO_2. However holes, which move via polaron hopping, are typically captured by deep holes in the SiO_2 or at the Si-SiO_2 interface, which results in fixed positive charge states. We denote the density of oxide charges by N_{ox}, the surface-current density by J_{surf}, and the density of interface traps as function of their energy E relative to the conduction band by $D_{it}(E)$ with units 1/(eV·cm^2). The interface traps, if exposed to an electric field, act as generation centers and generate a surface current.

For a realistic simulation and optimization of sensors, values of N_{ox}, N_{it}, the effective number of interface traps, and J_{surf} as function of dose are required. We therefore have ir-

*Corresponding author. Email: robert.klanner@desy.de.

radiated test structures from 4 different vendors (Canberra [14], CiS [15], Hamamatsu [16], Sintef [17]) built on high-ohmic n-type silicon (3 − 14 kΩ·cm), with different crystal orientations (⟨111⟩ and ⟨100⟩), and different dielectra (SiO_2 and SiO_2+Si_3N_4). The structures used were MOS Capacitors, MOS-C, and Gate-Controlled Diodes [18], GCD. The irradiations were performed at the "white" X-ray beam F4 at DORIS III, which had a mean energy of 12 keV and dose rates between 1 and 200 kGy/s [19, 20]. Irradiations were performed for dose values between 1 kGy and 1 GGy.

In order to determine $D_{it}(E)$, Thermal Dielectric Relaxation Current measurements, TDRC, on the MOS-C were made. In these measurements the MOS-C, biased in accumulation, was cooled down to a temperature of 10 K to freeze the electrons in the interface traps. Then the MOS-C was biased to deep depletion, heated up with a constant heating rate β = 0.183 K/s to 290 K, the current $I_{TDRC}(T)$ due to the release of the trapped electrons measured, and $D_{it}(E)$ extracted. To obtain quantitative results, the $D_{it}(E)$ spectrum was fitted by 3 Gauss functions [20]. From measurements with different heating rates β, the charge-carrier cross sections for the three levels were estimated. Following [21], this information was fed into an equivalent RC-circuit model and the voltage dependence of the capacitance/conductance, C/G-V, for different frequencies evaluated, assuming acceptor-like interface traps.

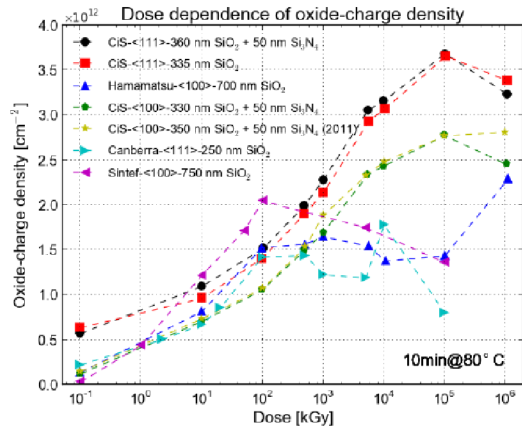

Figure 1: Dependence of the surface-charge density, N_{ox}, on X-ray dose obtained from measurements on MOS capacitors from 4 different vendors after annealing for 10 minutes at 80°C.

In order to determine N_{ox}, C/G-V measurements on the MOS-C for frequencies between 1 and 1000 kHz were made. N_{ox}, which just shifts the C/G-V curves along the V axis, has been derived from the voltage shift of the calculated 1 kHz C-V curve with respect to the data. After this shift the calculated C/G-V curves provide a fair description of the measurements for all frequencies and radiation doses.

Figure 1 shows the results for the thus determined values of N_{ox}. The CMOS-C had been annealed for 10 minutes at 80°C to reach a stable state with respect to short-term annealing. Up to an X-ray dose of approximately 100 kGy N_{ox} increases, and values of about $2 \cdot 10^{12}$ cm^{-2} are reached. Above this dose for some MOS-Cs N_{ox} saturates, for others it continues to increase. We have verified that the spread in N_{ox} for different MOS-Cs from the same producer is small, so that the large spread is attributed to the different technologies and crystal orientations.

For determining the surface-current densities, I-V measurements on Gate Controlled Diodes, GCD, were performed. The diodes were biased to −12 V, the voltage on the gate varied from accumulation via depletion to inversion, and the diode current measured. The surface-current density, J_{surf}, was obtained by dividing I_{surf}, the difference in current between depletion and accumulation, by the gate area. For the calculation of J_{surf} it has been assumed, that the entire gate area is depleted, which may not be correct for all GCDs at high currents. It has been estimated that in this way the value of J_{surf} could be underestimated by at most 50%. Figure 2 shows the results for J_{surf}. As for N_{ox}, the values of J_{surf} saturate at dose values between 1 and 10 MGy. The maximal values of J_{surf} vary between 1.5 and 6.5 μA/cm^2, which we again attribute to differences in technology. At higher doses J_{surf} decreases, which is not yet understood.

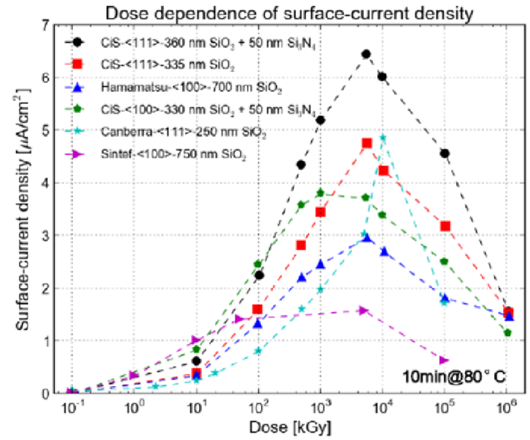

Figure 2: Dependence of the surface-current density J_{surf} on X-ray dose obtained from measurements on Gate Controlled Diodes from different vendors after annealing for 10 minutes at 80°C.

3. Sensor optimization

The results of the studies of the plasma effect have shown that for experiments with high instantaneous X-ray intensities, e.g. 10^4 X-ray photons per pulse in a 200 μm × 200 μm pixel, operating voltages well above 500 V are required for 500 μm thick sensors. The problem of reaching a high breakdown voltage for high radiation-induced oxide-charge densities is illustrated in Figure 3, which shows the electric field close to the Si-SiO_2 interface from a 2D TCAD simulation of a p^+n-strip sensor biased at 500 V for two values of N_{ox}. Whereas the maximal electric field 10 nm below the Si-SiO_2 interface is 50 kV/cm for $N_{ox} = 10^{11}$ cm^{-2}, it is 450 kV/cm for $N_{ox} = 2 \cdot 10^{12}$ cm^{-2}. The reason for this difference is, that the voltage difference between the readout strip and the accumulation layer increases with increasing oxide-charge density, and at the same time the width of the accumulation layer increases and extends below the metal

overhang. The result is a high electric field at the corner of the p^+ implant and a much reduced breakdown voltage.

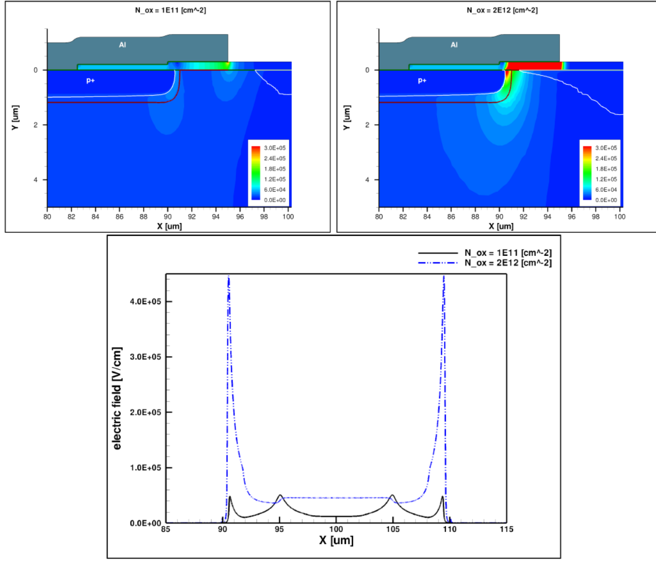

Figure 3: Influence of the oxide-charge density N_{ox} on the electric field close to the Si-SiO_2 interface. 2D simulation of a p^+ strip sensor. Top left: 2D field distribution for $N_{ox} = 10^{11}$ cm^{-2}. Top right: 2D field distribution for $N_{ox} = 2 \times 10^{12}$ cm^{-2}. Bottom: Electric field in the silicon 10 nm from the Si-SiO_2 interface for the two values of N_{ox}.

That X-ray radiation damage causes a significant reduction of the breakdown voltage, is also observed experimentally. Figure 4 shows for a sensor with a guard-ring structure consisting of one current-collection ring and 12 guard rings I-V curves for X-ray irradiations between 0 and 100 MGy. Whereas the non-irradiated sensor shows a "soft" breakdown around 900 V, the breakdown voltage for an irradiated sensor can be as low as 250 V. It should noted that this sensor has not been optimized for X-ray radiation hardness, and that the breakdown behavior in a dry (0.1% relative humidity) and a normal room atmosphere (40%) is similar.

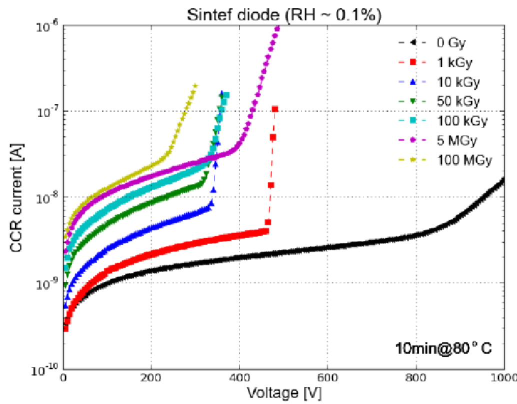

Figure 4: I-V characteristics of the Current Collection Ring of a Sintef sensor after annealing for 10 minutes at 80°C for different X-ray doses.

The optimization of the AGIPD sensor has been performed with the help of 2D and 3D TCAD simulations [22]. We first present the optimization of the layout of the guard-rings and then of the pixels. For the effective oxide-charge density, values up to $3 \cdot 10^{12}$ cm^{-2}, and for the current density, values up to 8 µA/cm^2 have been assumed.

For the optimization of the guard-ring structure, we first made a 2D simulation of a single p^+ strip on a 500 µm thick n-type crystal of 5 kΩ·cm resistivity. The p^+ strip, which was covered by aluminum overlapping the SiO_2, was surrounded by a Current Collection Ring, CCR, and an n^+-scribe-line implant. For three values of oxide-charge densities (1, 2, and $3 \cdot 10^{12}$ cm^{-2}) the I-V characteristics was simulated for different depths of the p^+ implant, dep, oxide thicknesses, t_{ox}, and aluminium overhang. The breakdown voltage V_{bd} was obtained from the I-V curve by the criterium $(dI/dV)/(I/V) = 10$.

Figure 5 shows the results. For $N_{ox} = 10^{12}$ cm^{-2} values for V_{bd} above 200 V are found for $t_{ox} > 300$ nm. For $3 \cdot 10^{12}$ cm^{-2} and $t_{ox} \gtrsim 300$ nm, V_{bd} drops to about 20 V. The reason is, that the silicon below the aluminium overhang depletes, and a high-field spike develops in the silicon at the corner of the p^+ implant, as shown in Figure 3. From the simulations we conclude, that a breakdown voltage of 70 V can be reached for an oxide thickness of 270 nm, a depth of the p^+ implant of 2.4 µm, and an aluminium overlap of 5 µm. We take these values as compromise between high breakdown voltage and technological feasibility.

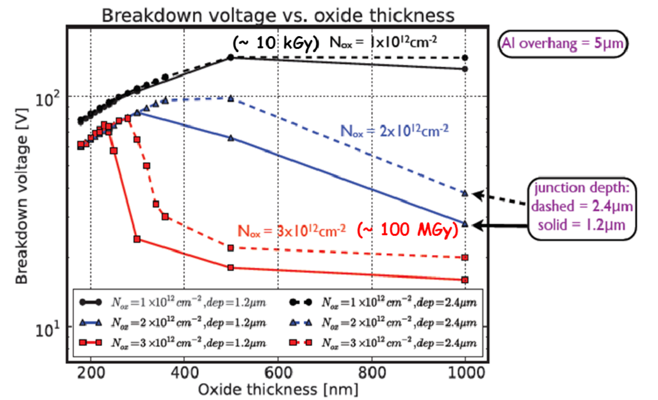

Figure 5: Breakdown voltage for a sensor surrounded by a CCR with zero GRs for different oxide charges, N_{ox}, two depths of the p^+ implant, dep, as function oxide thickness.

With $V_{bd} = 70$ V without a guard ring, GR, we estimate that 15 GRs will be required to reach a breakdown voltage approaching 1000 V. Next 2D simulations of a single strip and 15 GRs were performed. For $N_{ox} = 3 \cdot 10^{12}$ cm^{-2} and the parameters obtained from the zero-GR optimization, the spacing between the GRs, their p^+-implant widths, and the aluminium overhang towards the strip have been optimized for equal voltage drop between adjacent GRs and minimum required space. Finally, a simulation in cylindrical coordinates of a circular pixel and GR layout was performed to verify that the breakdown voltage is not significantly smaller at the corners.

For low surface-charge densities, care has to be taken that the depletion region does not touch the scribe line, as this would

result in an excessive current in the CCR. To verify that this is not the case, simulations were also made for $N_{ox} = 5 \cdot 10^{10}$ cm^{-2} as function of resistivity up to 12 kΩ·cm.

In the optimization of the pixel layout, breakdown voltage, inter-pixel capacitance and dark current have been considered. To estimate the inter-pixel capacitance and the dark current, the values from 2D simulations have been extrapolated to the 3D situation using empirical formulae. Given that accumulation layers form at the Si-SiO_2 interface, the inter-pixel capacitance depends only weakly on the distance between the p^+ implants of the pixels. As the dark current is given by $J_{surf} \cdot A_{dep}$, where A_{dep} is the area of the depleted Si-SiO_2 interface, the aluminum overhang and the gap between the p^+ implants should be small. A value of 20 μm for the gap and 5 μm for the overhang has been chosen.

Finally, a 3D simulation of a quarter of a pixel has been performed to verify the breakdown behavior and dark current. As symmetric boundary conditions were used, this corresponds to the simulation of a complete pixel sensor. The simulations show that, with the optimized parameters, the specifications of the AGIPD sensor, in particular a breakdown voltage above 900 V, a distance between the edges of the outer pixels and the cut edge of 1.2 mm, an inter-pixel capacitance below 500 fF, and a dark current for the sensor of less than 50 μm can be achieved for the values of N_{ox} and J_{surf}, which correspond to X-ray dose values between 0 and 1 GGy. The optimized design of a corner of the sensor is shown in Figure 6.

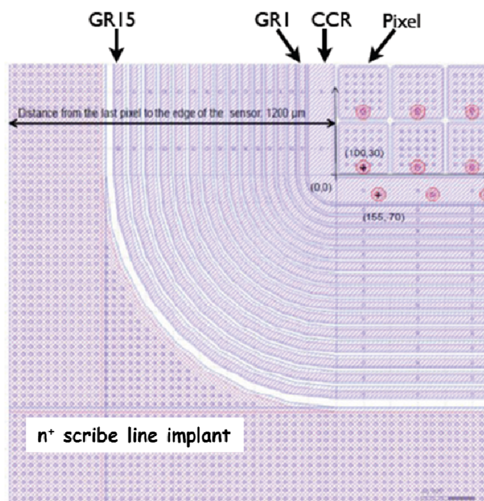

Figure 6: Layout of one corner of the AGIPD sensor. Starting from bottom left one sees the scribe lines, the n^+-scribe-line implant, the 15 guard rings, GR 15 - GR 1, the Current Collection Ring, CCR and 6 pixels.

4. Conclusions

Experimental results from the study of radiation damage on test structures and sensors built on high-ohmic n-type silicon for X-ray doses in the range 0 to 1 GGy have been presented. They have been implemented in TCAD simulations and used for optimizing the pixel sensor for the AGIPD (Adaptive Gain Integrating Pixel Detector) at the European X-Ray Free-Electron Laser. The simulations show that the specifications required for AGIPD can be met for X-ray dose values between 0 and 1 GGy.

Acknowledgements

R.K. thanks the organizers of the Vienna Conference of Instrumentation for the most pleasant, interesting, and exceedingly well organized conference. This work was performed within the AGIPD Project which is partially supported by the XFEL-Company. We would like to thank the AGIPD colleagues for the excellent collaboration. Support was also provided by the Helmholtz Alliance "Physics at the Terascale" and the German Ministry of Science, BMBF, through the Forschungsschwerpunkt "Particle Physics with the CMS-Experiment". J. Zhang is supported by the Marie Curie Initial Training Network "MC-PAD", and I. Pintilie gratefully acknowledges the financial support from the Romanian Authority for Scientific Research through the Project PCE 72/5.10.2011.

References

[1] M. Altarelli et al. (Eds.), *XFEL: The European X-Ray Free-Electron Laser, Technical Design Report*, Preprint DESY 2006-097, DESY, Hamburg 2006, ISBN 978-3-935702-17-1, and `http://www.xfel.eu/de/`.
[2] Th. Tschentscher et al., TECHNICAL NOTE XFEL.EU TN-2011-001 2011, DOI: 10.3204/XFEL.EU/TR-2011-001.
[3] H. Graafsma, 2009 JINST 4 P12011, DOI: 10.1088/1748-0221/4/12/P12011.
[4] R. Klanner et al., *Challenges for Silicon Pixel Sensors at the European XFEL*, to be published in Proceedings of RESMDD 13, subm. to Nucl. Instr. and Meth. A; arxiv:1212.5045.
[5] B. Henrich et al., Nucl. Instr. and Meth. A 663 (2011) S11-14, DOI: 10.1016/j.nima.2010.06.107.
[6] `http://hasylab.desy.de/instrumentation/detectors/projects/agipd/index_eng.html`.
[7] P.A. Tove and W. Seibt, Nucl. Instr. and Meth. 51 (1967) 261.
[8] J. Becker et al., Nucl. Instr. and Meth. A 615 (2010) 230-236, DOI: 10.1016/j.nima.2010.01.082.
[9] J. Becker, *Signal development in silicon sensors used for radiation detection*, PhD thesis, Universität Hamburg, DESY-THESIS-2010-33 (2010).
[10] T. Poehlsen, et al., Nucl. Instr. and Meth. A 700 (2013) 22-39, DOI: 10.1016/j.nima.2012.10.063.
[11] T. Poehlsen et al., *Time dependence of charge losses at the Si-SiO_2 interface in p^+n-silicon strip sensors*, to be published in Proceedings of PIXEL2012, submitted to Nucl. Instr. and Meth. A.
[12] T.R Oldham, *Ionizing Radiation effects in MOS Oxides, World Scientific Publishing Co.* (1999).
[13] H.J Barnaby, IEEE Trans. Nucl. Sci. 53 (2006) 3103.
[14] Canberra Industries Inc., `http://www.cismst.org`.
[15] CiS Forschungsinstitut für Mikrosensorik und Photovoltaikk GmbH, `http://www.cismst.org`.
[16] Hamamatsu Photonics, `http://www.hamamatsu.com`.
[17] Sintef ICT, `http://www.sintef.no`.
[18] A.S. Grove, *Physics and Technology of Semiconductor Devices*, John Wiley & Sons (1967).
[19] J. Zhang et al., 2012 JINST 7 C12012, DOI: 10.1088/1748-0221/7/12/C12012.
[20] J. Zhang et al., J. Synchrotron Rad. 19 (2012) 340-346, DOI: 10.1107/S0909049512002348.
[21] E.H. Nicollian and J.R. Brews, *MOS (Metal Oxide Semiconductor) Physics and Technology*, New York, Wiley-Interscience, 1982.
[22] J. Schwandt, E. Fretwurst, R. Klanner, J. Zhang, 2013 JINST 8 C12015, DOI: 10.1088/1748-0221/8/01/C01015.